



Optimization and modeling of *p*-nitroaniline removal from aqueous solutions in heterogeneous catalytic ozonation process using MgAl-layered double hydroxides (MgAl-LDH COP)

Mohammad Malakootian^a, Yousef Dadban Shahamat^b, Hakimeh Mahdizadeh^{c,*}

^aEnvironmental Health Engineering Research Center, Kerman University of Medical Sciences, Kerman, Iran, email: m.malakootian@yahoo.com

^bDepartment of Environmental Health Engineering, Faculty of Health, Environmental Health Research Center, Golestan University of Medical Sciences, Gorgan, Iran, email: dr.udadban@goums.ac.ir

^cEnvironmental Health Engineering Research Center, Kerman University of Medical Sciences, Kerman, Iran, Tel. +98 343 132 5128; Fax: +98 343 132 5435; email: H.mahdizadeh@kmu.ac.ir

Received 19 August 2020; Accepted 30 January 2021

ABSTRACT

p-nitroaniline (PNA) is a well-known acute oral, dermal, and inhalation toxin that has been reported as a priority toxic pollutant by the Environmental Protection Agency (EPA). In this study, MgAl-layered double hydroxides (MgAl-LDH) nanoparticles were prepared by a simple and fast co-precipitation method and used as a catalyst in the ozonation process to remove PNA from aqueous solutions. Next, the structure of the synthesized MgAl-LDH was investigated by X-ray diffraction pattern and field emission scanning electron microscopy-energy dispersive spectroscopy. The response surface methodology was used to investigate the effects of different parameters including reaction time, initial PNA concentration, pH, and LDH loading on the removal of PNA by MgAl-LDH catalytic ozonation process (MgAl-LDH COP). The highest removal efficiency of 91.5% was observed in optimum conditions as follows: initial PNA concentration of 162.5 mg/L, pH of 8.25, LDH loading of 750 mg/L, and reaction time of 70 min. The quadratic model was obtained with a high degree of fit. The removal values of COD and TOC were 77% and 68%, respectively. As a result, MgAl-LDH COP, as an excellent practical alternative, has a high performance in removing persistent compounds such as PNA from aqueous solutions.

Keywords: MgAl-layered double hydroxides; Catalytic ozonation; *p*-nitroaniline; Response surface methodology; Process optimization

1. Introduction

p-nitroaniline (PNA) is an important nitroaromatic compound that is widely used as an intermediate or precursor in the chemical synthesis of *p*-phenylenediamine, azo dyes, and glue, pesticides, disinfectants, antioxidants, antiseptic agents, drugs, and poultry [1]. PNA generally is introduced into the environment from different pathways such as industrial, military, and human activities.

This compound is a known acute oral, dermal, and inhalation toxin that has been reported as a priority toxic pollutant by Environmental Protection Agency (EPA) due to its toxicity, potentially carcinogenic, and mutagenic effects [1,2]. The presence of a stable nitro (NO₂) group in the aromatic ring increases its resistance to biodegradation under aerobic conditions, while the anaerobic degradation generates nitroso and hydroxylamines, which are famous

* Corresponding author.

as carcinogenic compounds [3,4]. Consequently, their presence in the environment is a big scientific concern.

Many conventional wastewater treatments and purification processes have been developed to remove these aromatic compounds. The major current processes in this respect include adsorption [1,5,6], Fenton oxidation [4], micro-electrolysis [2,7–9], biological treatment [10], and photochemical reactions [11].

However, there are some limiting factors to using conventional methods. For example, in biological processes, long times are required to remove these compounds due to their toxicity and non-biodegradability effects. In the adsorption techniques, pollutants are not destroyed and only are converted from one phase to another [11,12]. Currently, ozone as a strong oxidant with a redox potential of 2.07 V has drawn increasing attention in various environmental systems for its potential oxidation capacity [13,14]. Ozone reacts rapidly with organic substances in an aqueous solution in two ways: direct reaction with molecular ozone (O_3) or indirect reaction with the active radicals such as hydroxyl radicals ($\cdot OH$) generated by ozone decomposition. Hydroxyl radicals (redox potential of 2.33 V) react with most of the pollutants non-selectively, destroying them and converting them into harmless organic compounds such as CO_2 and H_2O [15]. O_3 molecules react selectively with the electron-rich compounds, so the reaction rate is quite slow for some other organic compounds such as those containing a nitro-group and increases energy consumption for ozone production [16,17]. These are examples of ozone application limitations for the direct removal of pollutants. As a consequence, the application of some combined oxidation technologies, such as ozone/UV, ozone/ H_2O_2 , and catalyst/ozone, can increase the production of hydroxyl radicals, leading to increased ozonation process efficiency and subsequent process cost reduction [18,19].

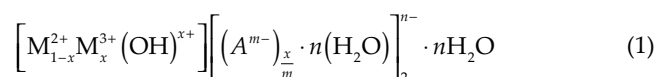
In the heterogeneous catalytic ozonation process (COP), the decomposition rate of refractory compounds in water increases due to the presence of a solid as a catalyst that produces destructive radicals [20,21]. Also, the mass transfer of ozone into liquid is improved at the COPs. Depending on the chemical nature of the catalyst used or the nature of the reactions, the COPs can be classified into heterogeneous and homogeneous processes, with the heterogeneous COPs having a higher degradation efficiency [15,20].

COPs have proved to be an effective process for removing non-biodegradation pollutants from aqueous environments. Ikhlaiq et al. [14] investigated the performance of the electrocoagulation process and COP using iron-loaded zeolite nanoparticles in the treatment of pharmaceutical wastewater. They could remove about 85% of COD and reported the removal efficiencies of 100% and 90% for pharmaceutical compounds such as enrofloxacin and amoxicillin, respectively.

So far, various heterogeneous catalysts have been investigated for COPs, including metal oxides like Fe_2O_3 , MnO_2 , Ce_2O_3 , WO_3 , TiO_2 , ZnO , CoO , Al_2O_3 , and MgO , zeolites, clay minerals, and activated carbon [13,14,20–22]. Recently, the synthesis and application of layered double hydroxides (LDHs) nanostructures in various fields, especially the water and wastewater treatment industry, has been considered as adsorbent and anionic exchanger due to their

excellent ion-exchange properties [23]. Among the various catalysts, LDH nanoparticles were chosen for this study because of their distinct properties such as layered structure, reactive interlayer space, wide chemical compositions, mechanical and chemical stability, ion-exchange, variable layer charge density, and colloidal properties [23,24].

LDHs are synthetic anionic clays having a two-dimensional (2D) lamellar structure consisting of both divalent M^{2+} and trivalent M^{3+} cations coordinated to six OH^- hydroxyl groups. The general formula of LDH can be expressed as bellow [23,25]:



where M^{2+} and M^{3+} represent a divalent metal (e.g., Mg^{2+} , Mn^{2+} , Co^{2+} , Fe^{2+} , Ni^{2+} , Cu^{2+} , and Zn^{2+}) and a trivalent metal (e.g., Al^{3+} , Mn^{3+} , Fe^{3+} , Cr^{3+} , Co^{3+}). Also, A^m denotes a general anion such as Cl^- , OH^- , CO_3^{2-} , NO_3^- , and SO_4^{2-} , etc. [23]. The schematic of the LDH structure is shown in Fig. 1.

Despite the growing interest in this field, relatively little attention has been paid to the use of LDH as catalysts in the ozonation process for refractory pollutants removal such as PNA. Because the ozonation process is costly in industrial applications, optimizing the process variables, and determining a statistical model can be very cost-effective [26].

Many experiments are required in the optimization of a multivariable process such as the ozonation technique with the one-factor method. Also, such methods do not demonstrate the combined effects of process variables and take a long time, which can be non-functional and unreliable in industrial applications [8,26,27]. Therefore, the issue of selecting an effective method for optimizing and modeling the process is very important. Response surface method (RSM) is a combination of statistical and mathematical methods used when the response variable is affected by several independent variables. Central composite design (CCD) is one of the most popular RSM methods [8,27]. CCD is used to determine optimal conditions expressing the influence of each independent variable [28]. Hence, the novelty of this work is mainly on the design, optimizing, and modeling of PNA removal from aqueous solutions by COPs using MgAl-LDH nanoparticles as a catalyst. Also, the raw materials applied in the preparation of MgAl-LDH are simple, non-toxic, and inexpensive mineral salts. The process variables including initial PNA concentration, LDH dose, initial pH, and reaction time were optimized by the CCD method and the best mathematical model was selected. This process has a high potential for the degradation of refractory pollutants such as PNA and can be suggested and widely used in the water and wastewater treatment plants.

2. Materials and methods

PNA ($C_6H_6N_2O_2$; 99.5%), magnesium chloride hexahydrate ($MgCl_2 \cdot 6H_2O$; 99.9%), aluminium chloride hexahydrate ($AlCl_3 \cdot 6H_2O$; 99.9%), potassium iodide (KI; 99.5%), sodium hydroxide (NaOH; 99.5%), sulfuric acid (H_2SO_4 ; 99.5%), sodium thiosulfate ($Na_2S_2O_3$; 99.5%), starch ($(C_6H_{10}O_5)_n - (H_2O)$;

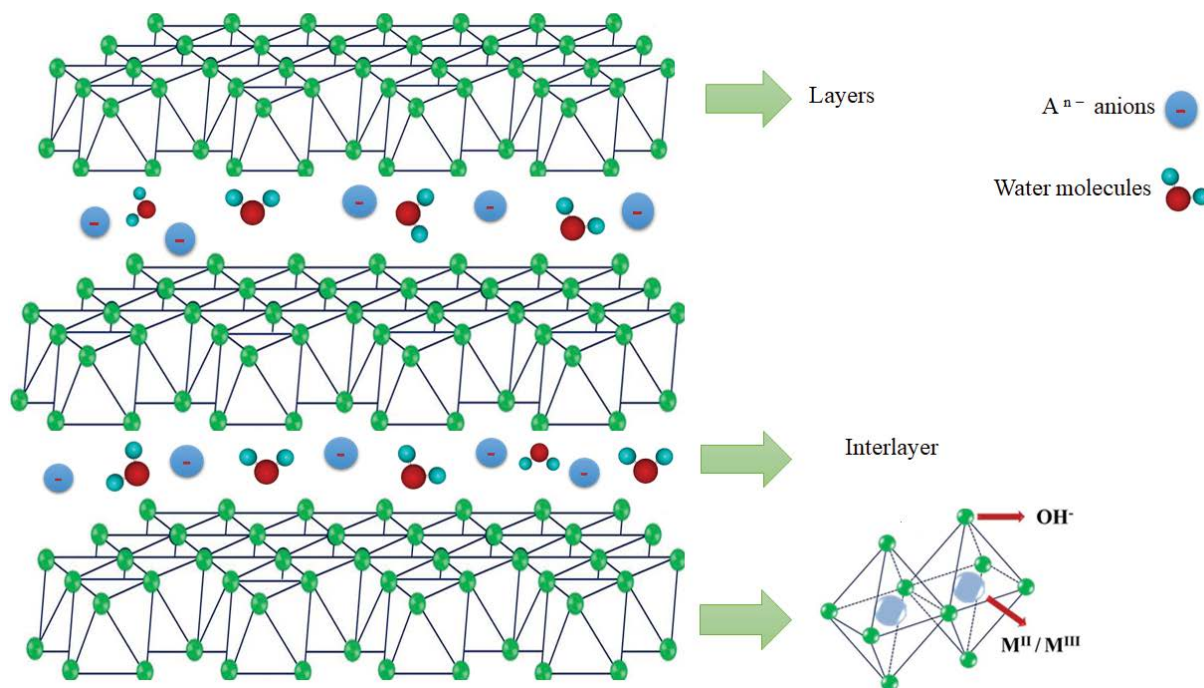


Fig. 1. Schematic of the layered double hydroxides (LDHs) structure.

99.5%), methanol (CH_3OH ; 99%), and *tert*-butanol ($(\text{CH}_3)_3\text{COH}$; 99%) were all purchased from Merck, Germany.

2.1. Preparation of MgAl-LDH nanocatalyst

MgAl-LDH nanocatalyst was synthesized by the co-precipitation method at room temperature ($23^\circ\text{C} \pm 5^\circ\text{C}$). A solution (50 mL) containing 10.165 g of magnesium chloride hexahydrate and 9.63 g of aluminum chloride hexahydrate was added dropwise under vigorous stirring to an aqueous solution of NaOH (4 M, 50 mL). The obtained suspension was transferred into a Teflon-lined autoclave (50 mL in volume) and maintained at 180°C for 48 h. The as-prepared product was centrifuged and washed several times with deionized water. Finally, the white precipitate was dried at 60°C overnight to obtain MgAl-LDH nanocatalyst [29,30].

2.2. Catalytic ozonation reactor and operation

The COP experiments were carried out using a pyrex cylindrical reactor of 300 mL, equipped with a sintered-glass diffuser at the bottom operating in the semi-batch mode. Ozone was produced using an ARDA ozone generator (model MOG). Silicone hoses, which are resistant to ozone gas, were used to the joints between reactor components. The amount of ozone gas entering the COP reactor was set at 2.55 mg/min by the Iodometric method [31]. To prevent health damage, KI (2%) solutions were used to destroy excess ozone molecules. To increase the efficiency of the ozonation process, the MgAl-LDH nanoparticles synthesized by the co-precipitation method were used as a catalyst in the COP process. A schematic of the COP reactor is shown in Fig. 2.

2.3. Experimental design

A CCD with four independent variables was used to investigate the effect of the initial concentration of LDH, PNA concentration, reaction time, and initial solution pH and their interactions on responses (i.e., PNA removal efficiency). The ranges of the independent variables were selected based on the literature review. Based on the CCD matrix, a total of 30 experimental runs were designed to calculate the coefficients of the second-order polynomial regression model for independent factors. The independent variables were selected based on the previous literature.

Each variable was studied at five levels: $-\alpha$, -1 , 0 , $+1$, and $+\alpha$. The actual and coded levels used for CCD design are shown in Table 1.

The quadratic polynomial response model for predicting the optimal point is expressed by Eq. (2) [26,32].

$$Y = \beta_0 + \sum_{i=1}^k \beta_i X_i + \sum_{i=1}^k \beta_{ii} X_i^2 + \sum_{i=1}^{k-1} \sum_{j=i+1}^k \beta_{ij} X_i X_j \quad (2)$$

where Y , β_0 , β_i , β_{ii} , β_{ij} , X_i , X_j , and k are the response variable (i.e., PNA removal efficiency), the constant coefficient, the linear coefficients, the quadratic coefficients, the interaction coefficients, the coded independent variables, and the number of input variables, respectively [26,28].

The analysis of variance (ANOVA) was carried out to determine the effect of independent variables on the response variable and the optimal conditions by Design Expert 8.0 software.

To determine the effect of the radical scavenger on the PNA removal, under optimum conditions, *tert*-butanol (80 mM) was added into PNA synthetic solution to examine its effect on PNA removal [15,33].

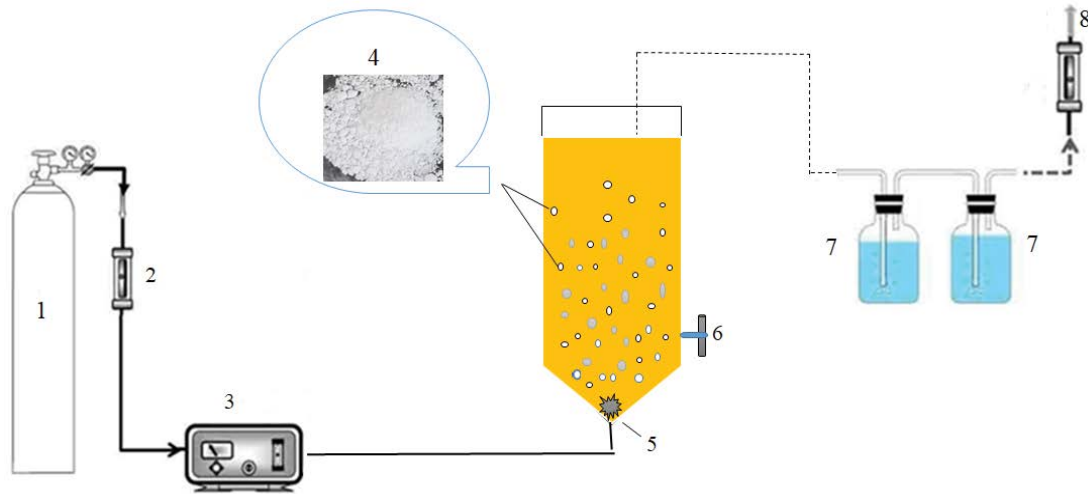


Fig. 2. Schematic of the COP reactor containing MgAl-LDH nanocatalyst for PNA removal: (1) O₂ capsule, (2) rotameter, (3) ozone generator, (4) Mg-Al LDH nanoparticles, (5) air distributor, (6) sampling valve, (7) gas trapper (KI solution), and (8) gas outlet.

Table 1
Coded and real values of the independent variables used for CCD design

Independent variable	Coded symbol	Levels of variables					Unit of variables
		$-\alpha$	-1	0	+1	$+\alpha$	
LDH dose	X_1	0	250	500	750	1,000	mg/L
pH	X_2	3	4.75	6.5	8.25	10	–
Initial PNA concentration	X_3	50	87.5	125	162.5	200	mg/L
Reaction time	X_4	10	30	50	70	90	min

2.4. Analytical method

The residues of PNA in the solution were analyzed by high-performance liquid chromatography (HPLC). The HPLC analyses were performed with an HPLC device (Waters E600, USA) equipped with a UV absorbance detector at the wavelength of 381 nm and a C₁₈ column (5 μm particle size, 250 mm × 4.6 mm). The HPLC was run with a mixture of methanol/water (40/60, v/v) mobile phase at 0.8 mL/min and μL injection volume [3,34]. The pH of solutions was adjusted by the addition of 1.0 N of either H₂SO₄ or NaOH solutions. All experiments were carried out at room temperature (23°C ± 5°C).

The process was evaluated by measuring the reduction of chemical oxygen demand (COD) and total organic carbon (TOC) amounts under optimum conditions. A TOC analyzer (Jena-C3100, Germany) was used to determine the TOC amount. COD analyses were carried out using the recycled distillation based on the C5220 method, the 20th edition of the “Standard Methods for the Examination of Water and Wastewater” book [35].

2.5. Characterization

The field emission scanning electron microscopy-energy dispersive spectroscopy (FESEM-EDAX; TESCAN mira3, Czech Republic) was performed to observe the

surface morphology and the size of synthesized MgAl-LDH nanoparticles.

To characterize the structural properties (characterization of constituent phases and crystalline size) of nanoparticles, X-ray diffraction (XRD) patterns were recorded in the diffraction angle range $2\theta = 10^\circ\text{--}80^\circ$ by a Rigaku Ultima IV (made in Japan).

2.6. pH point of zero charges

The pH point of zero charges (pH_{pzc}) measurement of the prepared LDH nanoparticles was performed by the solid addition method. Briefly, the initial pH values of 100 mL of the KCl solution (0.1 mol/L) were adjusted at different pH values (2–12). Subsequently, 0.01 g of the MgAl-LDH nanoparticles were added to each solution. The obtained suspensions were agitated for 48 h until an equilibrium pH value was reached, followed by measuring the pH of the final solution. The initial pH (pH_i) was plotted against the final pH (pH_f). The intersection point of $\text{pH}_i = \text{pH}_f$ was chosen as pH_{zpc} [36,37].

3. Results and discussion

3.1. Model fitting and statistical analysis

The design matrix for the different experimental conditions and the response to experiments proposed by CCD for PNA removal are given in Table S1.

Based on these results, a second-order polynomial regression equation in terms of actual factors was obtained that demonstrates the empirical relationships between the response and independent variables in the coded units as below:

$$Y = 40.03418 + 0.02437X_1 - 0.44608X_2 - 0.01762X_3 + 0.78506X_4 + 0.00013X_1X_3 - 0.00023X_1X_4 + 0.01390X_2X_3 + 0.00278X_3X_4 - 0.00002X_1^2 - 0.00117X_3^2 - 0.00377X_4^2 \quad (3)$$

ANOVA analysis was carried out to evaluate the adequacy of the model. The results are shown in Table 2.

From the ANOVA of the empirical second-order polynomial model, the p -value for the model is <0.0001 , indicating that the model is highly significant. According to the correlation coefficient ($R^2 = 0.9967$), there is a 0.0033% chance that the total variation could not be explained by the empirical model for the degradation of PNA by LDH COPs. Therefore, this model was chosen as the best model to predict the PNA removal efficiency.

Usually, the significant variables are ranked based on the F - or p -value parameters with a 95% confidence level. The higher F -value and lower p -value indicate more significance of the variable [8,27]. Based on the results of F -values,

LDH dose, the reaction time, initial pH of the solution, and PNA concentration were the most effective parameters in COP for PNA degradation. Factors with a p -value ≤ 0.05 were considered significant and retained in the model.

As shown in Table 2, the coefficient of variation (CV) of 1.14% was obtained for this model. CV is an indicator used to measure the dispersion distribution of statistical data. This coefficient indicates the degree of precision with which the factors are compared [27]. The higher value of the CV indicates low reliability of the model with the experimental data and the lower value represents more reliability of the model [27,28]. Therefore, this model can be suggested to predict the removal efficiency of PNA within the limits of the experimental variables by LDH COP.

In the study of Dehghani et al. [32], the adsorption rate of bisphenol A on the surface of powdered and granular activated carbon was modeled by CCD-RSM. The results showed a good fit between quadratic model predictions with experimental values, such that R^2 of 0.9992 and 0.9997 were obtained for powdered and granular activated carbon, respectively.

Fig. 3 shows the model diagnostics plots. The data points in a normal plot are linear when the studentized residuals are normally distributed (Fig. 3a). In this Fig. 3, all points are relatively close to the straight line and confirm

Table 2
ANOVA results of response surface quadratic model for PNA removal

Source	Sum of squares	df	Mean square	F -value	p -value	
Model	3,445.88	14	246.13	324.98	<0.0001	Significant
X_1 -LDH dose	208.86	1	208.86	275.76	<0.0001	
X_2 -pH	9.37	1	9.37	12.38	0.0031	
X_3 -PNA concentration	8.64	1	8.64	11.41	0.0041	
X_4 -time	2,943.73	1	2,943.73	3,886.67	<0.0001	
X_1X_2	0.4225	1	0.4225	0.5578	0.4667	
X_1X_3	23.52	1	23.52	31.06	<0.0001	
X_1X_4	21.62	1	21.62	28.55	<0.0001	
X_2X_3	13.32	1	13.32	17.59	0.0008	
X_2X_4	3.42	1	3.42	4.52	0.0505	
X_3X_4	69.72	1	69.72	92.06	<0.0001	
X_1^2	40.88	1	40.88	53.98	<0.0001	
X_2^2	0.3219	1	0.3219	0.4250	0.5243	
X_3^2	74.30	1	74.30	98.10	<0.0001	
X_4^2	62.40	1	62.40	82.39	<0.0001	
Residual	11.36	15	0.7574			
Lack of fit	9.59	10	0.9590	2.71	0.1416	Not significant
Pure error	1.77	5	0.3542			
Core total	3,457.24	29				
Standard deviation				0.8703		
Mean				76.57		
C.V.%				1.14		
R-squared				0.9967		
Adj. R-squared				0.9936		
Pred. R-squared				0.9833		
Adeq. precision				71.9877		

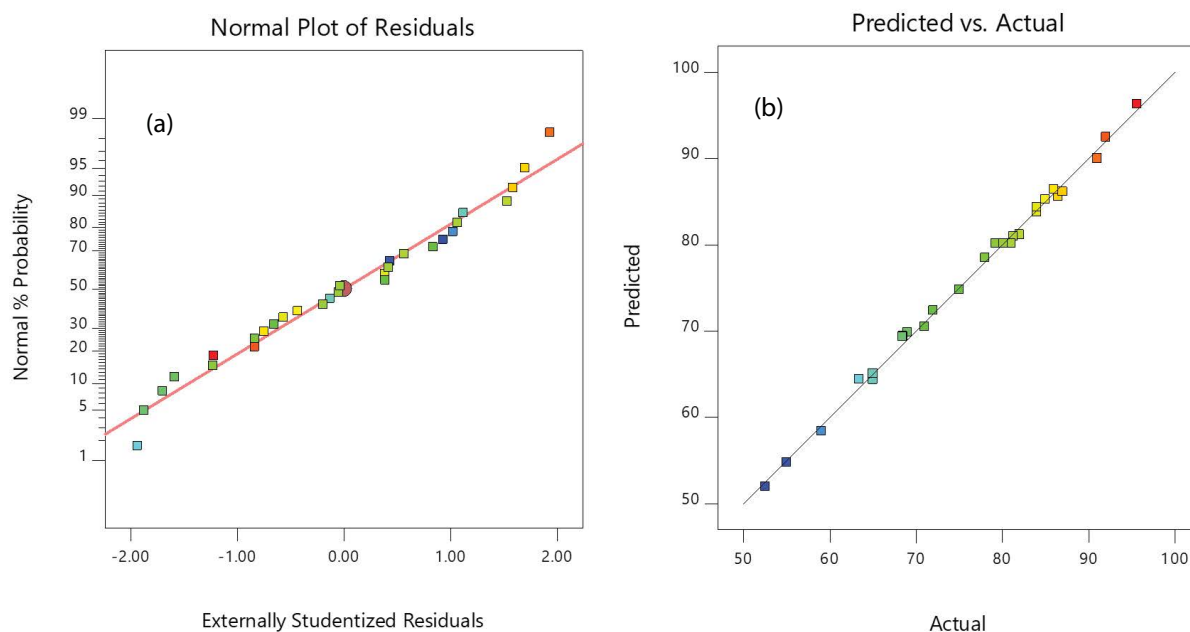


Fig. 3. Model diagnostics plots: (a) normal probability plot of studentized residuals and (b) predicted vs. actual values of PNA removal.

that the data are normally distributed. Fig. 3b represents the correlation between the observed and predicted values of the PNA removal by LDH COPs. As can be seen, the points are placed very close to the straight line indicating the validity and adequacy of the predicted model.

3.2. Optimum conditions of the model

The optimized conditions for PNA removal using MgAl-LDH COP were obtained by response optimizer. The values of optimized independent variables are presented in Table 3.

The main objective of optimizing the independent variables of this study was to achieve the highest PNA removal by MgAl-LDH COP. Under optimal conditions, the predicted and actual efficiency of the model for PNA removal were achieved to be 92.475% and 91.50%, respectively, suggesting a strong correlation between predicted and observed values of this model.

3.3. MgAl-LDH characterization

3.3.1. XRD analysis of MgAl-LDH nanoparticles

The crystal structure and phase purity of the as-prepared MgAl-LDH nanoparticles were investigated using the XRD analysis. The XRD pattern of MgAl-LDH nanoparticles is illustrated in Fig. 4.

The XRD pattern of the MgAl-LDH showed the characteristic peaks of LDH structure, described in the literature. The diffraction peaks of crystal planes at $2\theta = 11.51^\circ$, 14.48° , 23.17° , 28.17° , 31.70° , 35.07° , 60.72° , and 62.04° are related to the MgAl-LDH structure of the nanoparticles. Moreover, the sharp and strong diffraction peaks demonstrate ordered and regular stacking of LDH layers. The original main peaks at 2θ of 11.51° , 23.17° , and 35.08° are related

to Mg and Al mixed-layer minerals (JCPDS 96-210-2793). The weak and broad peaks at 2θ of 14.48° , 28.17° , 38.37° , 60.72° , and 62.04° derived from γ -AlOOH (Boehmite structure, JCPDS 96-901-2252 and 96-901-2248,) were similarly detected in the XRD pattern of MgAl-LDH. The peaks at 2θ of 60.72° and $2\theta = 62.04^\circ$ can be attributed to the arrangement of the ions along the plane of the host layer [29,38].

3.3.2. FESEM with EDAX analysis

The surface morphology of the MgAl-LDH nanoparticles was investigated using the FESEM analysis. Fig. 5 demonstrates the FESEM images of synthesized LDH. As can be seen, they are agglomerated fine particles with a spherical shape and average particle size of 45.8 nm. EDAX gives the chemical composition of the as-prepared MgAl-LDH (Fig. 6). EDAX element distribution reveals the presence of Mg, Al, O, and Cl that confirm the purity of the synthesized MgAl-LDH compound.

3.4. Effect of operational parameters on PNA removal efficiency

The three-dimensional (3D) response surfaces and linear plots in Fig. 7 indicate the effect of operational parameters including LDH dose (mg/L), PNA initial concentration (mg/L), pH, and reaction time (min) on PNA removal efficiency by MgAl-LDH COP. Using response surface plots allows predicting the removal efficiency of PNA in different values of parameters.

Figs. 7a and b demonstrate the effect of LDH dose on PNA removal efficiency ($R\%$) at central point values of other parameters. According to ANOVA analyses, the LDH concentration with a high F -value had a significant effect on the response y (PNA removal) compared to other variables such as pH and PNA concentration. It is obvious

Table 3
Values of optimized independent variables

PNA removal efficiency (%)		LDH dose (mg/L)	pH	PNA concentration (mg/L)	Reaction time (min)	Desirability
Observed	Predicted					
91.50	92.475	750.000	8.250	162.500	70.000	0.927

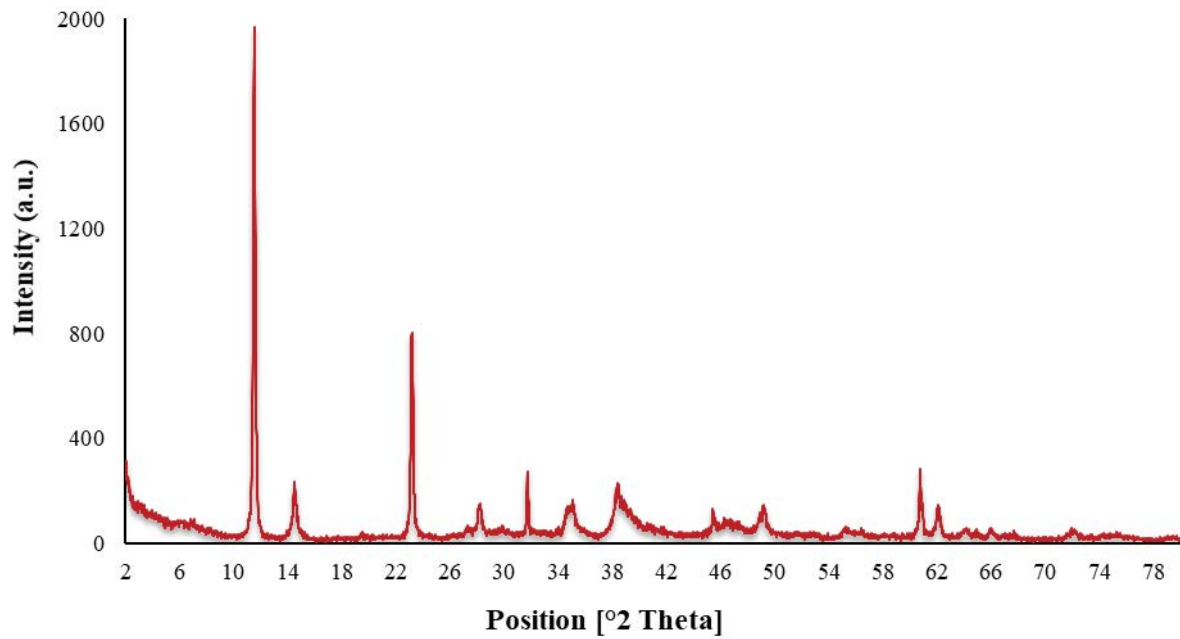


Fig. 4. XRD pattern of MgAl-LDH nanoparticles.

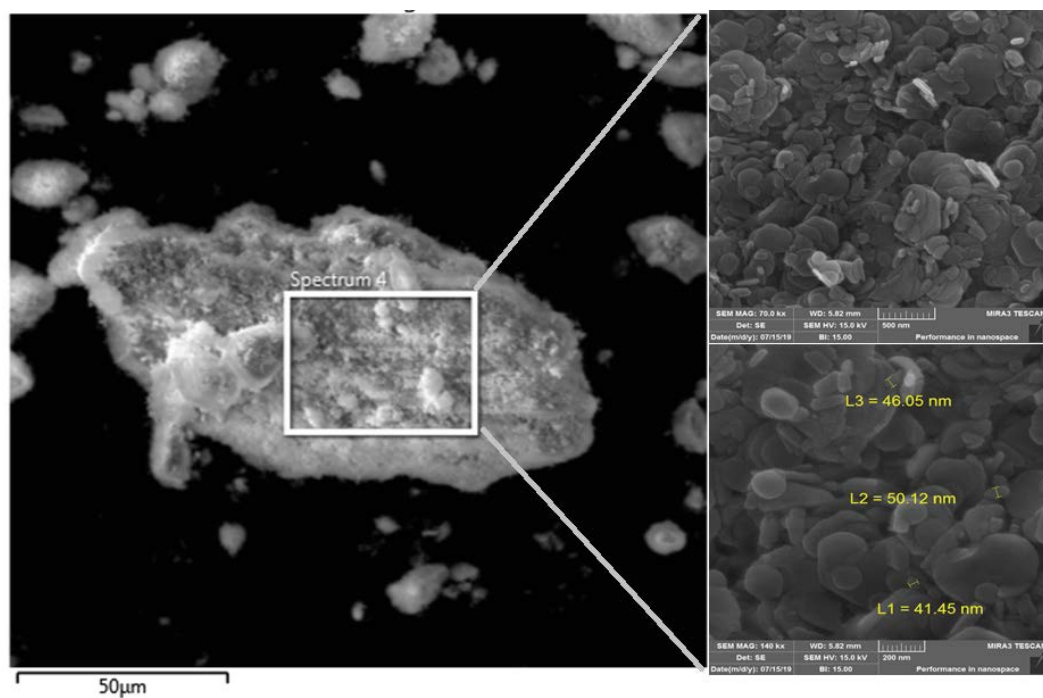


Fig. 5. FESEM images of MgAl-LDH nanoparticles.

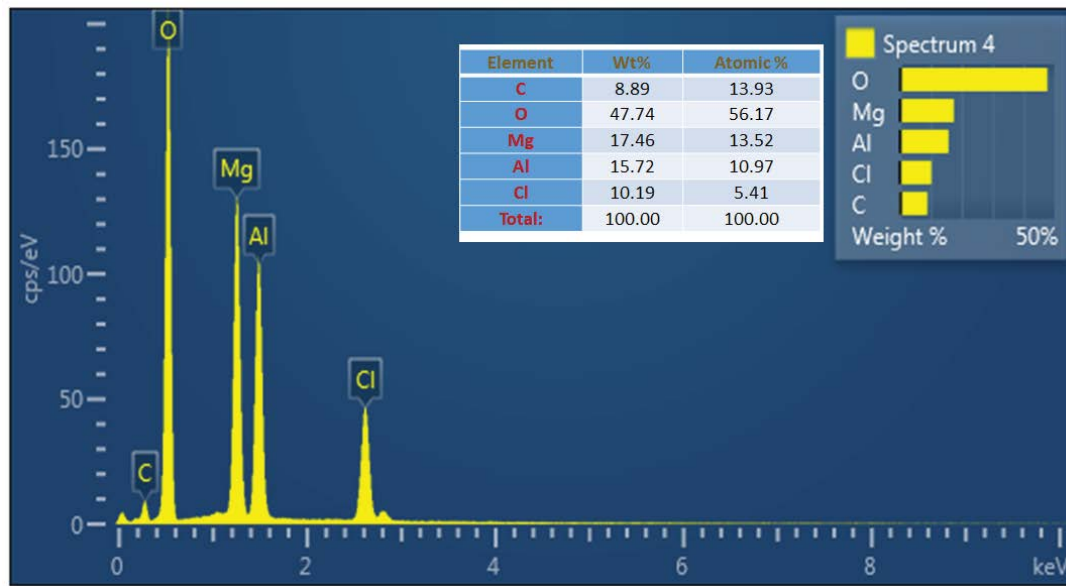
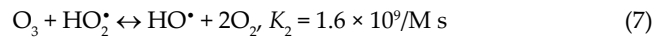
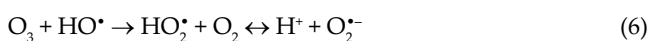
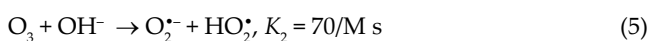
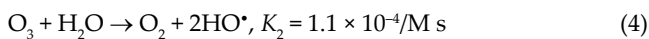


Fig. 6. EDAX elemental spectrum and (inset) elemental composites of MgAl-LDH nanoparticles.

from Figs. 7a and b that with increasing LDH nanoparticles concentration from 0 to 750 mg/L and reaction time to 90 min, the PNA removal efficiency increased rapidly. The further increase in LDH leads to a reduction in removal efficiency. To demonstrate the catalytic activity of MgAl-LDH on PNA removal, four control processes were investigated under the same experimental conditions including pH: 8.25, initial PNA concentration: 162.5, temperature: $23^{\circ}\text{C} \pm 5^{\circ}\text{C}$: (1) COP, (2) single ozonation process (SOP), (3) adsorption process without the presence of ozone, and (4) aeration process without the presence of LDH. The results are shown in Fig. 8.

As shown in Fig. 8, the PNA removal efficiency in the presence of LDH nanoparticles by MgAl-LDH COP was much more significant compared to the processes of SOP, adsorption, and aeration. As can be inferred from this Fig. 8, the effect of air on PNA removal was completely negligible. In the adsorption process, the maximum removal efficiency of PNA was achieved to be 15% at 20 min then remained constant. In SOP and COP, with increasing reaction time from 0 to 70 min, the removal efficiency of PNA increased rapidly such that it was 65% and 91.5% were obtained, respectively, at end of reaction time. Therefore, the high removal of PNA in the COP can be due to degradation but not adsorption.

Due to the presence of LDH nanoparticles as a solid substance in the ozonation process, the generation of $\cdot\text{OH}$ radicals derived from ozone destruction enhanced, leading to an increase in the removal efficiency of PNA [25,39]. The chain reactions of ozone destruction in the presence of the catalyst can be described by Eqs. (4)–(8) [21,39]:



Increasing the PNA removal efficiency with an increase in LDH concentration in the COP can be attributed to the increase in the number of active sites at the surface of the nanoparticles in reaction with ozone in solution [25,39]. As a result, the transfer of ozone from the gas phase to the solution, and the rate of ozone destruction also increase. Thus, increasing ozone decomposition leads to an enhance in the concentration of radical hydroxyl in the surface and volume of the liquid, and eventually increasing the process efficiency and the decomposition of organic compounds into minerals such as CO_2 and H_2O [25,39].

However, with further increasing LDH concentration from 750 to 1,000 mg/L, PNA removal was not significantly enhanced. An explanation is that using excessive LDH nanoparticles might reduce the effective contact of O_3 molecules with the catalyst surface and thus reduce the concentration of O_3 per unit area, leading to a decrease in the process efficiency [15,23].

Figs. 7c and d represent the effect of solution pH on PNA removal efficiency (%R) at central point values of other parameters. As can be seen in this figure, and according to ANOVA analyses, increasing the initial pH from 3 to 10 does not have an obvious effect on the PNA removal. Therefore, the removal efficiency of the process is not so pH-dependent. However, the removal efficiency increased slightly with the increase in initial pH. This can be related to the effect of pH on the properties of the catalyst surface and the ozone transfer from the gas phase to the solution and ozone destruction [25,39]. At alkaline pH, ozone decomposition generates free active radicals (such as superoxide ion ($\text{O}_2^{\cdot-}$), radical HO_2^{\cdot} , and especially OH^{\cdot} radicals), which are extremely oxidizing species that selectively react with organic and inorganic compounds in aqueous solutions [14,17].

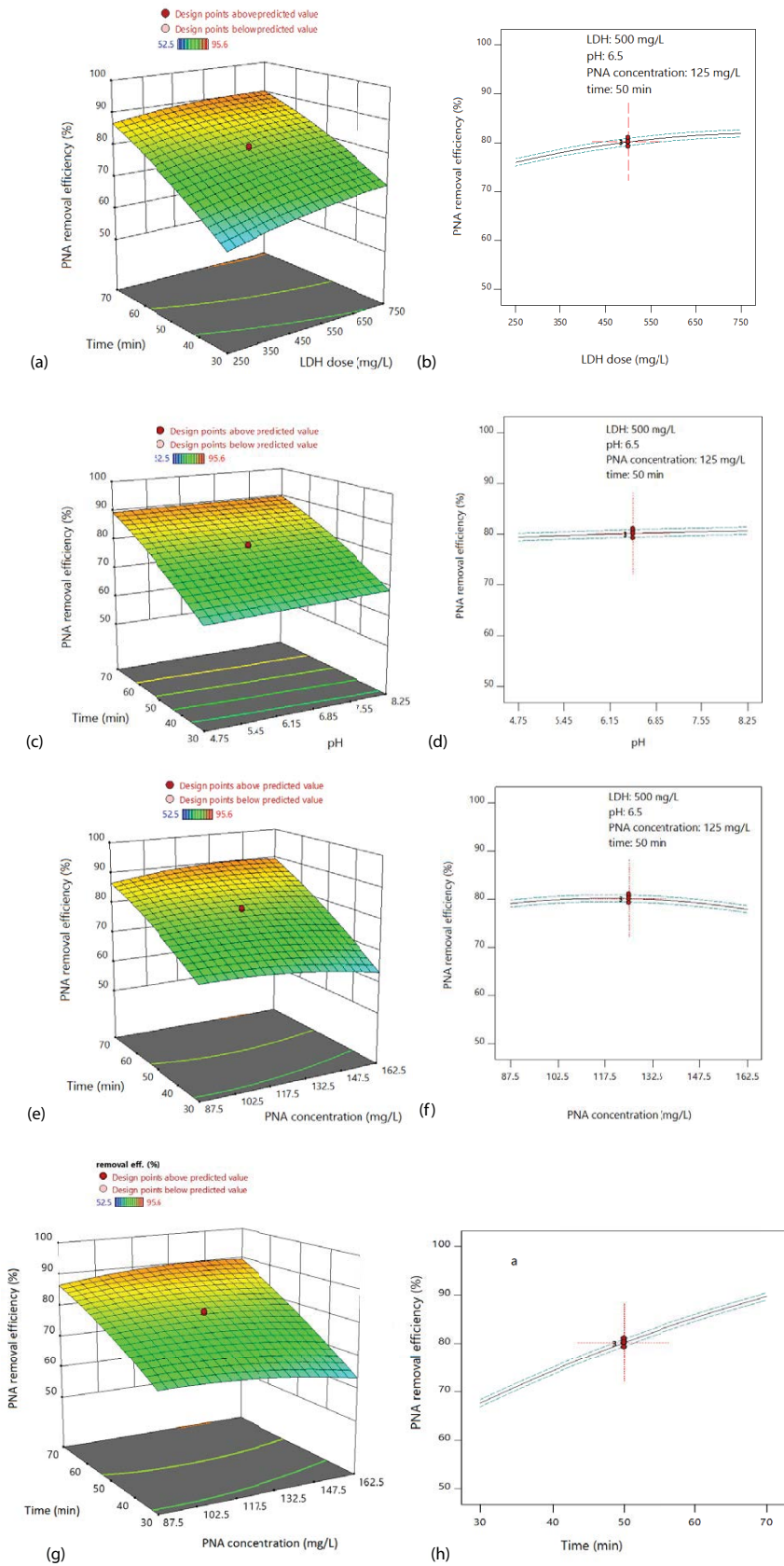


Fig. 7. Effect of operational parameters on the response (PNA removal efficiency) at central point values of other parameters (LDH dose: 500 mg/L, pH: 8.25, PNA concentration: 125 mg/L, reaction time: 50 min, and temperature: 23°C ± 5°C).

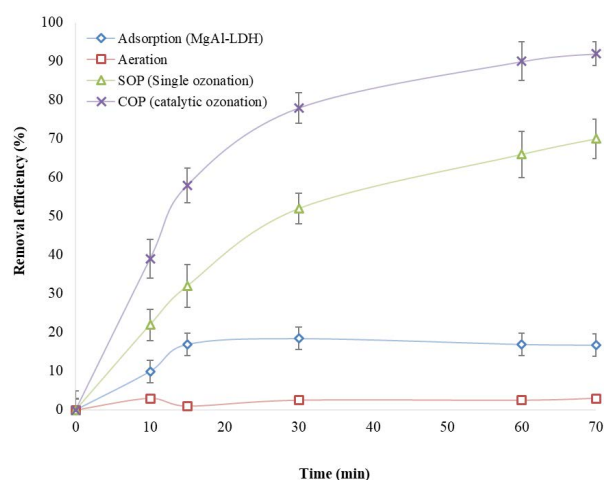


Fig. 8. Effect of different processes on the removal efficiency of PNA (pH: 8.25, PNA concentration: 162.5, and temperature: $23^{\circ}\text{C} \pm 5^{\circ}\text{C}$).

In contrast, ozone molecules are stable at acidic pH and thus react with compounds through selective reactions. The lower efficiency of the ozonation in acidic or natural conditions is a negative drawback of this process [15,18,40]. The persistent compounds such as PNA, which react slowly with ozone molecules, decompose unselectively at high pH values. In this study, due to the presence of LDH nanoparticles as a catalyst in the ozonation process, more free active radicals were formed via the decomposition of ozone molecules, which would enhance the process efficiency under acidic, natural, and alkaline conditions [23,25]. Besides, the high removal of PNA in acidic pH can be related to pH_{pzc} of MgAl-LDH nanoparticles. The pH_{pzc} of MgAl-LDH was determined to be 7.5 by the solid addition method. At pH below pH_{zpc} , the surface of LDH nanoparticles was protonated, thereby increasing the chance of adsorption of PNA ions [21,23].

These results are in general agreement with the results of sulfamethoxazole removal in the COP with $\text{Fe}_3\text{O}_4/\text{Co}_3\text{O}_4$ composites conducted by Chen and Wang [41]. Also, Yan et al. [42] in a study on nitrobenzene removal in COP with Si-doped $\alpha\text{-Fe}_2\text{O}_3$, reported that with the increase in solution pH from 5.5 to 6.5 and 7.5, nitrobenzene removal increased from 79.8% to 85% and 90%, respectively. Similar results have been reported in the literature [14,15,43].

Ikhlq et al. [13] compared the removal efficiency of methylene blue by COP, ozonation, and adsorption by iron nanoparticles. At pH = 3 and under acidic conditions, Fenton process, and pH = 10 under alkaline conditions, the efficiency of the ozonation process was maximum, but COP had a good performance under all acidic, alkaline, and neutral conditions. COP was effective in all pH ranges. Other similar results have been reported elsewhere [23,24,44].

Figs. 7e and f show the effect of PNA initial concentration on the response y (%R) at central point values of other parameters. In the advanced oxidation process (AOP), the pollutant concentration in aqueous solutions plays an important role in the oxidation efficiency and the synergistic effects of AOP processes such as SOP and COP

[22,23]. Rey et al. [45] investigated the mineralization of metoprolol by photocatalytic ozonation process and found that the synergistic effects of the process were greater at the higher pollutant concentrations compared with low concentrations.

As can be seen from Fig. 7f, and according to ANOVA analyses, the initial concentration of PNA negatively affects the response (removal efficiency). Therefore, the removal efficiency decreased slightly with increasing initial concentration of PNA. This could be ascribed to the insufficiency of ozone molecules compared to PNA molecules in the solution [12,46]. Increasing the pollutant concentration leads to a reduction in the number of active sites to stimulate. Besides, a greater amount of intermediates can be generated in higher pollutant concentrations, leading to an increase in ozone consumption occurs [12,46]. The presence of a catalyst in the ozonation process can reduce ozone consumption and increase the performance of the process. Similar results were reported in previous studies. For example, Alinejad et al. [47] prepared the MgO nanoparticles and used them for degrading methotrexate drug from aqueous solutions by COP. They reported that due to the low $\cdot\text{OH}$ radical production from O_3 depletion in the higher drug concentrations, degradation efficiency decreased [47].

Figs. 7g and h show the effect of contact time on the response y (%R) at central point values of other parameters. According to ANOVA analyses, contact time with the highest F -value had a considerable effect on the PNA removal. As can be seen from Figs. 7g and h, the removal efficiency of PNA gradually increased with reaction time such that after a reaction time of 90 min under the optimum conditions, the PNA removal efficiency reached 91.5%. The UV/vis spectrum of PNA with a maximum wavelength of 381 nm is presented in Fig. 9, indicating the trend of PNA degradation with increased reaction time in MgAl-LDH COP.

3.5. Investigation on mineralization of PNA

To investigate the performance of this process in the degradation of PNA, we performed TOC and COD analyses under optimum operating conditions for five different processes, that is, SOP, MgAl-LDH COP, aeration, and adsorption. Because the ozone gas was produced from dry air, the aeration process was also tested. As can be seen from the obtained results (Fig. 10), for the initial concentration of 125 mg/L of PNA and under the optimum conditions, the initial COD and TOC values of the PNA sample are 8 and 5.5 g/L, respectively. Also, the figure shows that using the SOP process and after 120 min, COD and TOC decreased by 65% and 59%, respectively. The removal efficiency of COD and TOC was 77% and 68% in the ozonation process in the presence of MgAl-LDH at a concentration of 750 mg/L (MgAl-LDH COP), respectively. The maximum removal efficiency of COD and TOC in the adsorption process was 9.5% and 6%, respectively, which could be ignored during the COP. Meanwhile, the aeration process had no significant effect on COD removal and TOC removal. These results confirmed that the addition of MgAl-LDH nanoparticles enhanced the process performance. In a study conducted by Huang et al. [25], Ni-Fe layered double hydroxides (Ni-Fe

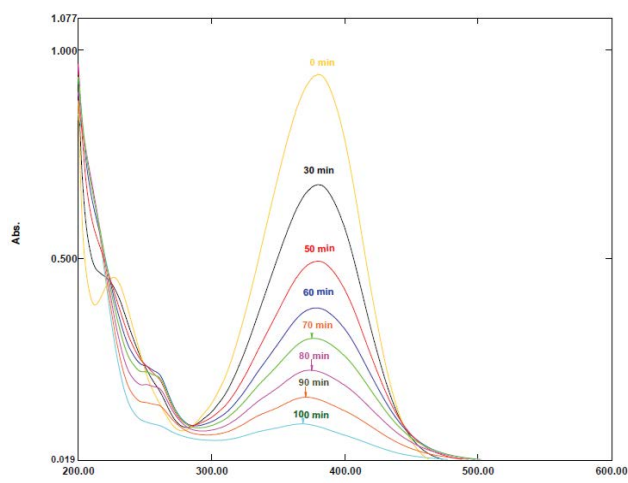


Fig. 9. UV/vis spectrum of PNA.

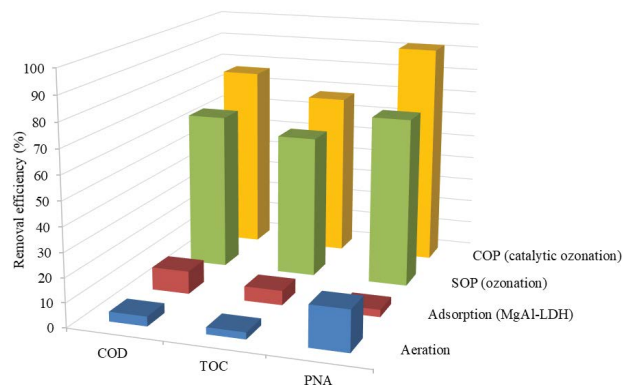


Fig. 10. COD and TOC removal efficiency in PNA degradation (pH: 8.25, time: 90 min, initial PNA concentration: 162.5 mg/L, and temperature: 23°C ± 5°C).

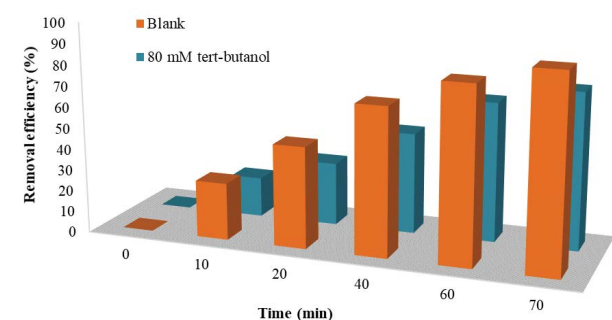


Fig. 11. Effect of *tert*-butanol as a radical scavenger on PNA removal in the MgAl-LDH/COP reactor (pH: 8.25, LDH dosage: 750 mg/L, initial PNA concentration: 162.5 mg/L, and temperature: 23°C ± 5°C).

LDHs) nanoparticles were synthesized and used as a catalyst in heterogeneous catalytic ozonation to remove bisphenol A (BPA) and other organic compounds in secondary effluent.

Under optimal conditions (catalyst dosage: 0.3 g/L; aqueous ozone concentration: 9.0 mg/L; initial pH: 8.2; initial BPA concentration: 10 mg/L), BPA in the secondary effluent was completely removed and the final efficiency of TOC and COD removal was 56% and 68%, respectively.

In a study conducted by El Hassani et al. [23], the catalytic activity of Ni-based layered double hydroxides (Ni-LDHs) nanoparticles was investigated for methyl orange (MO) degradation. Under optimized conditions (i.e., $T = 20^{\circ}\text{C}$, pH = 9, ozone flow rate = 109 mg/h, catalyst dosage = 1 g/L, initial concentration of MO = 500 mg/L, COD initial = 620 mg/L, and after 60 min reaction), the COD removal was obtained 72% in the COP, while it was only 30% in the non-catalytic ozonation. Similar results were obtained from the literature [2,12,41].

3.6. Radical scavenger impact

The effect of *tert*-butanol as a radical scavenger on the PNA removal was determined under optimal conditions. The results are shown in Fig. 11.

Adding *tert*-butanol as a radical scavenger diminished the efficiency of PNA removal from 91.5% to 75% at the end of the reaction time (70 min). The free radicals produced from ozone destruction reactions (Eqs. (4)–(8)) have high chemical activity and can eliminate the carbon chain of organic compounds [33,48]. *Tert*-butanol can scavenge these radicals and inhibit their degrading effects. However, it was found that the presence of radical scavengers lowered the removal efficiency of the COP process. This observation is in good agreement with other studies that have reported the negative effect of radical scavengers on the formation of hydroxyl radicals [33,49,50]. Ma et al. [33] investigated the effect of radical scavengers such as *tert*-butanol and bicarbonate on the catalytic ozonation of atrazine in the presence of Mn nanoparticles. They reported that the presence of radical scavengers has a very strong influence on the removal reduction of atrazine, even at low concentrations.

4. Conclusion

In this study, the removal efficiency of PNA in the COP was investigated using MgAl-layered double hydroxides (MgAl-LDH) nanoparticles as a catalyst. MgAl-LDH nanoparticles were synthesized by a simple and fast co-precipitation method. MgAl-LDH catalyst was characterized by XRD and FESEM-EDAX analyses. Next, effects of process variables including initial PNA concentration, LDH dose, initial pH, and reaction time were studied on the removal of PNA by the MgAl-LDH COP. The CCD was used for the optimization and modeling of the process. After optimizing the variables, it was tried to evaluate the process performance, the TOC and COD analyses under optimum conditions. The highest removal efficiency of 91.5% was observed in optimum conditions as follows: initial PNA concentration = 162.5 mg/L, pH = 8.25, LDH dose = 750 mg/L, and reaction time = 70 min. The quadratic model was obtained with a high degree of fit. The removal of COD and TOC were 77% and 68%, respectively. Due to the short contact time with ozone and high efficiency, this technique has more economical justification compared to other PNA ozonation

methods. However, more economic-based studies are needed in this regard. Overall, MgAl-LDH COP, as an excellent practical alternative, has a high performance in removing persistent compounds such as PNA from aqueous solutions.

Acknowledgments

This research was conducted at the Environmental Health Engineering Research Center and was sponsored by the Vice-Chancellor for Research and Technology of Kerman University of Medical Sciences. The authors take this opportunity to express their gratitude for the support and assistance extended by the facilitators during the research.

References

- [1] M.E. Mahmoud, A.E. Abdou, A.K. Shehata, H.M. Header, E.A. Hamed, Behavior of γ -Al₂O₃-bonded-3-chloropropyl-trimethoxysilane nanosorbent toward potential binding and removal of 4-nitroaniline and 2-amino-3-nitro-pyridine from water, *J. Mol. Liq.*, 224 (2016) 1358–1369.
- [2] M. Malakootian, M. Pournamdari, A. Asadipour, H. Mahdizadeh, Degradation and removal of *p*-nitroaniline from aqueous solutions using a novel semi-fluid Fe/charcoal micro-electrolysis reactor, *Korean J. Chem. Eng.*, 36 (2019) 217–225.
- [3] A. Saupe, High-rate biodegradation of 3-and 4-nitroaniline, *Chemosphere*, 39 (1999) 2325–2346.
- [4] J.H. Sun, S.P. Sun, M.H. Fan, H.Q. Guo, L.P. Qiao, R.X. Sun, A kinetic study on the degradation of *p*-nitroaniline by Fenton oxidation process, *J. Hazard. Mater.*, 148 (2007) 172–177.
- [5] M. Malakootian, M.H. Ehrampoush, H. Mahdizadeh, A. Golpayegani, Comparison studies of raw and oxidized multi-walled carbon nanotubes H₂SO₄/HNO₃ to remove *p*-nitroaniline from aqueous solution, *J. Water Chem. Technol.*, 40 (2018) 327–333.
- [6] M. Afsharnia, H. Biglari, A. Javid, F. Zabihi, Removal of reactive black 5 dye from aqueous solutions by adsorption onto activated carbon of grape seed, *Iran. J. Health Sci.*, 5 (2017) 48–61.
- [7] M. Malakootian, H. Mahdizadeh, M. Khavari, A. Nasiri, M.A. Gharaghani, M. Khatami, E. Sahle-Demessie, R.S. Varma, Efficiency of novel Fe/charcoal/ultrasonic micro-electrolysis strategy in the removal of Acid Red 18 from aqueous solutions, *J. Environ. Chem. Eng.*, 8 (2020) 103553, doi: 10.1016/j.jece.2019.103553.
- [8] H. Mahdizadeh, M. Malakootian, Optimization of ciprofloxacin removal from aqueous solutions by a novel semi-fluid Fe/charcoal micro-electrolysis reactor using response surface methodology, *Process Saf. Environ. Prot.*, 123 (2019) 299–308.
- [9] M. Malakootian, K. Kannan, M.A. Gharaghani, A. Dehdarirad, A. Nasiri, Y.D. Shahamat, H. Mahdizadeh, Removal of metronidazole from wastewater by Fe/charcoal micro electrolysis fluidized bed reactor, *J. Environ. Chem. Eng.*, 7 (2019) 103457, doi: 10.1016/j.jece.2019.103457.
- [10] A. Khalid, M. Arshad, D.E. Crowley, Biodegradation potential of pure and mixed bacterial cultures for removal of 4-nitroaniline from textile dye wastewater, *Water Res.*, 43 (2009) 1110–1116.
- [11] J. Mohamadiyan, G. Shams-Khoramabadi, S.A. Mousavi, B. Kamarehie, Y. Dadban Shahamat, H. Godini, Aniline degradation using advanced oxidation process by UV/Peroxy disulfate from aqueous solution, *Int. J. Eng.*, 30 (2017) 684–690.
- [12] M. Malakootian, M. Khatami, H. Mahdizadeh, A. Nasiri, M. Amiri Gharaghani, A study on the photocatalytic degradation of *p*-nitroaniline on glass plates by thermo-immobilized ZnO nanoparticle, *Inorg. Nano-Metal Chem.*, 50 (2020) 124–135.
- [13] A. Ikhlaiq, H.M.S. Munir, A. Khan, F. Javed, K.S. Joya, Comparative study of catalytic ozonation and Fenton-like processes using iron-loaded rice husk ash as catalyst for the removal of methylene blue in wastewater, *Ozone Sci. Eng.*, 41 (2019) 250–260.
- [14] A. Ikhlaiq, F. Javed, A. Akram, A. Rehman, F. Qi, M. Javed, M.J. Mehdi, F. Waheed, S. Naveed, H.A. Aziz, et al., Synergic catalytic ozonation and electroflocculation process for the treatment of veterinary pharmaceutical wastewater in a hybrid reactor, *J. Water Process Eng.*, 38 (2020) 101597, doi: 10.1016/j.jwpe.2020.101597.
- [15] Y. Dadban Shahamat, M. Farzadkia, S. Nasser, A.H. Mahvi, M. Gholami, A. Esrafil, Magnetic heterogeneous catalytic ozonation: a new removal method for phenol in industrial wastewater, *J. Environ. Health Sci. Eng.*, 12 (2014) 1–12, doi: 10.1186/2052-336X-12-50.
- [16] Y. Dadban Shahamat, M.A. Zazouli, M.R. Zare, N. Mengelizadeh, Catalytic degradation of diclofenac from aqueous solutions using peroxymonosulfate activated by magnetic MWCNTs-CoFe₂O₄ nanoparticles, *RSC Adv.*, 9 (2019) 16496–16508.
- [17] C. Gottschalk, J.A. Libra, A. Saupe, *Ozonation of Water and Waste Water: A Practical Guide to Understanding Ozone and its Applications*, John Wiley & Sons, Germany, 2009.
- [18] K. Ikehata, Y. Li, Chapter 5 - Ozone-Based Processes, S.C. Ameta, R. Ameta, Eds., *Advanced Oxidation Processes for Wastewater Treatment*, Elsevier S&T Book, Academic Press, Cambridge, MA, ISBN: 978-0-128104996, 2018, pp. 115–134.
- [19] M. Malakootian, M. Amiri Gharaghani, A. Dehdarirad, M. Khatami, M. Ahmadian, M.R. Heidari, H. Mahdizadeh, ZnO nanoparticles immobilized on the surface of stones to study the removal efficiency of 4-nitroaniline by the hybrid advanced oxidation process (UV/ZnO/O₃), *J. Mol. Struct.*, 1176 (2019) 766–776.
- [20] A. Ikhlaiq, M. Anis, F. Javed, H. Ghani, H.M.S. Munir, K. Ijaz, Catalytic ozonation for the treatment of municipal wastewater by iron loaded zeolite A, *Desal. Water Treat.*, 152 (2019) 108–115.
- [21] H. Mahdizadeh, A. Nasiri, M.A. Gharaghani, G. Yazdanpanah, Hybrid UV/COP advanced oxidation process using ZnO as a catalyst immobilized on a stone surface for degradation of acid red 18 dye, *MethodsX*, 7 (2020) 101118, doi: 10.1016/j.mex.2020.101118.
- [22] M. Kermani, F. Bahrami Asl, M. Farzadkia, A. Esrafil, S. Salahshour Arian, M. Khazaei, Y.D. Shahamat, D. Zeynalzadeh, Heterogeneous catalytic ozonation by Nano-MgO is better than sole ozonation for metronidazole degradation, toxicity reduction, and biodegradability improvement, *Desal. Water Treat.*, 57 (2016) 16435–16444.
- [23] K. El Hassani, D. Kalnina, M. Turks, B.H. Beakou, A. Anouar, Enhanced degradation of an azo dye by catalytic ozonation over Ni-containing layered double hydroxide nanocatalyst, *Sep. Purif. Technol.*, 210 (2019) 764–774.
- [24] Y. Qi, C. Guo, X. Xu, B. Gao, Q. Yue, B. Jiang, Z. Qian, C. Wang, Y. Zhang, Co/Fe and Co/Al layered double oxides ozone catalyst for the deep degradation of aniline: preparation, characterization and kinetic model, *Sci. Total Environ.*, 715 (2020) 136982, doi: 10.1016/j.scitotenv.2020.136982.
- [25] Y. Huang, T. Yang, M. Liang, Y. Wang, Z. Xu, D. Zhang, L. Li, Ni-Fe layered double hydroxides catalyzed ozonation of synthetic wastewater containing Bisphenol A and municipal secondary effluent, *Chemosphere*, 235 (2019) 143–152.
- [26] M. Afsharnia, M. Shams, M. Ghasemi, H. Biglar, S. Salari, A. Moteallemi, Modeling and optimization of fluoride adsorption from aqueous samples by ammonium aluminium sulfate using response surface methodology (RSM), *Res. Rep. Fluoride*, 52 (2019) 299–318.
- [27] A. Aghaeinejad-Meybodi, A. Ebadi, S. Shafiee, A.R. Khataee, M. Rostampour, Modeling and optimization of antidepressant drug fluoxetine removal in aqueous media by ozone/H₂O₂ process: comparison of central composite design and artificial neural network approaches, *J. Taiwan Inst. Chem. Eng.*, 48 (2015) 40–48.
- [28] A.A. Salarian, Z. Hami, N. Mirzaei, S.M. Mohseni, A. Asadi, H. Bahrami, M. Vosoughi, A. Alinejad, M.-R. Zareh, N-doped TiO₂ nanosheets for photocatalytic degradation and mineralization of diazinon under simulated solar irradiation:

- optimization and modeling using a response surface methodology, *J. Mol. Liq.*, 220 (2016) 183–191.
- [29] M. Zhang, B. Gao, Y. Yao, M. Inyang, Phosphate removal ability of biochar/MgAl-LDH ultra-fine composites prepared by liquid-phase deposition, *Chemosphere*, 92 (2013) 1042–1047.
- [30] B. Zhu, L. Chen, T. Yan, J. Xu, Y. Wang, M. Chen, H. Jiang, Fabrication of $\text{Fe}_3\text{O}_4/\text{MgAl}$ -layered double hydroxide magnetic composites for the effective removal of Orange II from wastewater, *Water Sci. Technol.*, 78 (2018) 1179–1188.
- [31] C.M. Birdsall, A.C. Jenkins, E. Spadinger, Iodometric determination of ozone, *Anal. Chem.*, 24 (1952) 662–664.
- [32] M.H. Dehghani, R.R. Karri, Z.T. Yeganeh, A.H. Mahvi, H. Nourmoradi, M. Salari, A. Zarei, M. Sillanpää, Statistical modelling of endocrine disrupting compounds adsorption onto activated carbon prepared from wood using CCD-RSM and DE hybrid evolutionary optimization framework: comparison of linear vs non-linear isotherm and kinetic parameters, *J. Mol. Liq.*, 302 (2020) 112526, doi: 10.1016/j.molliq.2020.112526.
- [33] J. Ma, N.J.D. Graham, Degradation of atrazine by manganese-catalysed ozonation—influence of radical scavengers, *Water Res.*, 34 (2000) 3822–3828.
- [34] Y.S. Zhao, C. Sun, J.Q. Sun, R. Zhou, Kinetic modeling and efficiency of sulfate radical-based oxidation to remove *p*-nitroaniline from wastewater by persulfate/ Fe_3O_4 nanoparticles process, *Sep. Purif. Technol.*, 142 (2015) 182–188.
- [35] A.D. Eaton, M.A.H. Franson, American Water Works Association, Water Environment Federation, Standard Methods for the Examination of Water and Wastewater, American Public Health Association, 2005.
- [36] D. Datta, Ö. Kerkez Kuyumcu, Ş.S. Bayazit, M. Abdel Salam, Adsorptive removal of malachite green and Rhodamine B dyes on Fe_3O_4 /activated carbon composite, *J. Dispersion Sci. Technol.*, 38 (2017) 1556–1562.
- [37] M. Malakootian, A. Nasiri, H. Mahdizadeh, Preparation of CoFe_2O_4 /activated carbon@chitosan as a new magnetic nanobiocomposite for adsorption of ciprofloxacin in aqueous solutions, *Water Sci. Technol.*, 78 (2018) 2158–2170.
- [38] R-r. Shan, L.-g. Yan, K. Yang, S.-y. Yu, Y.-f. Hao, H.-q. Yu, B. Du, Magnetic $\text{Fe}_3\text{O}_4/\text{MgAl}$ -LDH composite for effective removal of three red dyes from aqueous solution, *Chem. Eng. J.*, 252 (2014) 38–46.
- [39] Y. Huang, M. Luo, Z. Xu, D. Zhang, L. Li, Catalytic ozonation of organic contaminants in petrochemical wastewater with iron-nickel foam as catalyst, *Sep. Purif. Technol.*, 211 (2019) 269–278.
- [40] H. Zhang, Y. He, L. Lai, G. Yao, B. Lai, Catalytic ozonation of Bisphenol A in aqueous solution by $\text{Fe}_3\text{O}_4\text{-MnO}_2$ magnetic composites: performance, transformation pathways and mechanism, *Sep. Purif. Technol.*, 245 (2020) 116449, doi: 10.1016/j.seppur.2019.116449.
- [41] H. Chen, J. Wang, Catalytic ozonation of sulfamethoxazole over $\text{Fe}_3\text{O}_4/\text{Co}_3\text{O}_4$ composites, *Chemosphere*, 234 (2019) 14–24.
- [42] P. Yan, J. Shen, L. Yuan, J. Kang, B. Wang, S. Zhao, Z. Chen, Catalytic ozonation by Si-doped $\alpha\text{-Fe}_2\text{O}_3$ for the removal of nitrobenzene in aqueous solution, *Sep. Purif. Technol.*, 228 (2019) 115766, doi: 10.1016/j.seppur.2019.115766.
- [43] M. Farzadkia, Y. Dadban Shahamat, S. Nasser, A.H. Mahvi, M. Gholami, A. Shahryari, Catalytic ozonation of phenolic wastewater: identification and toxicity of intermediates, *J. Eng.*, 2014 (2014) 1–11, doi: 10.1155/2014/520929.
- [44] A. Ikhlaq, F. Javed, R. Sohail, M. Kazmi, A. Rehman, F. Qi, Solar photo-catalytic ozonation on γ -alumina for the removal of dyes in wastewater, *Int. J. Environ. Sci. Technol.*, (2020) 1–8, doi: 10.1007/s13762-020-02940-5.
- [45] A. Rey, D.H. Quinones, P.M. Álvarez, F.J. Beltrán, P.K. Plucinski, Simulated solar-light assisted photocatalytic ozonation of metoprolol over titania-coated magnetic activated carbon, *Appl. Catal., B*, 111 (2012) 246–253.
- [46] Y. Dadban Shahamat, M. Sadeghi, A. Shahryari, N. Okhovat, F. Bahrami Asl, M.M. Baneshi, Heterogeneous catalytic ozonation of 2, 4-dinitrophenol in aqueous solution by magnetic carbonaceous nanocomposite: catalytic activity and mechanism, *Desal. Water Treat.*, 57 (2016) 20447–2056.
- [47] A. Alinejad, H. Akbari, M. Ghaderpoori, A.K. Jaihooni, A. Adibzadeh, Catalytic ozonation process using a MgO nanocatalyst to degrade methotrexate from aqueous solutions and cytotoxicity studies in human lung epithelial cells (A549) after treatment, *RSC Adv.*, 9 (2019) 8204–8214.
- [48] Y. Wang, H. Cao, C. Chen, Y. Xie, H. Sun, X. Duan, S. Wang, Metal-free catalytic ozonation on surface-engineered graphene: microwave reduction and heteroatom doping, *Chem. Eng. J.*, 355 (2019) 118–129.
- [49] A. Ikhlaq, D.R. Brown, B. Kasprzyk-Hordern, Catalytic ozonation for the removal of organic contaminants in water on alumina, *Appl. Catal., B*, 165 (2015) 408–418.
- [50] A.G. Gonçalves, J.J.M. Orfão, M.F.R. Pereira, Catalytic ozonation of sulphamethoxazole in the presence of carbon materials: catalytic performance and reaction pathways, *J. Hazard. Mater.*, 239 (2012) 167–174.

Supplementary information

Table S1
Experimental and predicted values of PNA removal

Run	Std	Factor 1	Factor 2	Factor 3	Factor 4	Response (observed)	Response (predicted)
		X ₁ : LDH dose mg/L	X ₂ : pH	X ₃ : PNA concentration mg/L	X ₄ : reaction time min	Y = removal efficiency %	Removal efficiency %
1	6	250	4.75	87.5	30	65	64.375
2	8	750	4.75	87.5	30	69	69.85
3	1	250	8.25	87.5	30	63.4	64.4
4	11	750	8.25	87.5	30	71	70.525
5	19	250	4.75	162.5	30	55	54.75
6	25	750	4.75	162.5	30	65	65.075
7	16	250	8.25	162.5	30	59	58.425
8	17	750	8.25	162.5	30	68.5	69.4
9	3	250	4.75	87.5	70	86.5	85.6
10	15	750	4.75	87.5	70	86	86.425
11	27	250	8.25	87.5	70	84	83.775
12	24	750	8.25	87.5	70	85	85.25
13	12	250	4.75	162.5	70	84	84.325
14	7	750	4.75	162.5	70	91	90
15	22	250	8.25	162.5	70	87	86.15
16	21	750	8.25	162.5	70	92	92.475
17	10	0	6.5	125	50	68.4	69.375
18	13	1,000	6.5	125	50	82	81.175
19	9	500	3	125	50	78	78.475
20	29	500	10	125	50	81.3	80.975
21	2	500	6.5	50	50	75	74.775
22	5	500	6.5	200	50	72	72.375
23	18	500	6.5	125	10	52.5	51.975
24	4	500	6.5	125	90	95.6	96.275
25	28	500	6.5	125	50	80.5	80.15833
26	30	500	6.5	125	50	81	80.15833
27	20	500	6.5	125	50	80	80.15833
28	23	500	6.5	125	50	80.12	80.15833
29	14	500	6.5	125	50	79.2	80.15833
30	26	500	6.5	125	50	80.13	80.15833